Proceedings of the 2013 IEEE/SICE International Symposium on System Integration, Kobe International Conference Center, Kobe, Japan, December 15-17,

Design of a Kangaroo Robot with Dynamic Jogging Locomotion

Guan-Horng Liu, Hou-Yi Lin, Huai-Yu Lin, Shao-Tuan Chen, and Pei-Chun Lin

Abstract—**Based on the inspiration of the kangaroo's locomotion, we report on the development of a kangaroo robot with dynamic locomotion. Not like bipeds, quadrupeds, or hexapods which use multi legs for locomotion, the kangaroo usually moves two legs in phase, which resides in a very unique class of locomotion as the monopod. Though special, the research about its continuous forward locomotion is very limited. In this work, the center of mass locomotion of the robot is designed to move according to the spring loaded inverted pendulum (SLIP) with rolling contact, based on the fact that the SLIP is widely used as the model for legged animal's dynamic locomotion. To compensate the possible body pitch variation, the robot is equipped with an active tail for pitch variation compensation, like the kangaroo does. The robot is empirically built, and various design issues and strategies are addressed. Finally, the experimental evaluation is executed to validate the performance of the design of the robot with dynamic locomotion.**

I. Introduction

BIO-INSPIRED robotics is an emerging branch of the robotics. Based on the concept of learning from nature, robotic researchers try to develop or improve the mechanical structure, control algorithm, and overall locomotion behavior of the robots by incorporating untraditional and bio-inspired gradients.

One of the popular categories of bio-inspired robotics is legged robotics, where the researchers work on analyzing legged behavior or developing robots which can run dynamically or negotiate with rough terrain like animal does. For example, BigDog and LS3 built by Boston Dynamics (BDI) have great mobility [1]. Tekken II developed by Kimura et al. has spring-mass-damping systems between the leg joints to stimulate viscoelastic characteristics of muscle tissue [2]. Poulakakis et al. conducted a series of experiments on Scout II, to excite it dynamically stable bounding under complex situations via simple control laws [3]. Sprawlita series from Stanford can run dynamically [4] and its motion pattern is similar to the behavior of spring loaded inverted pendulum (SLIP), which is used by most of legged animals [5]. RHex from UMich has very simple morphology, yet having versatile behaviors [6]. Cheetah from MIT has very dedicate morphology design [7]. Besides quadrupeds and hexapods, now some biped robots can also perform dynamic running (i.e., with flight phase); however, the comparison of its running motion to the SLIP model is still very limited.

This work is supported by National Science Council (NSC), Taiwan, under contract NSC 100-2628-E-002-021-MY3.

All authors are with Department of Mechanical Engineering, National Taiwan University (NTU), No.1 Roosevelt Rd. Sec.4, Taipei, Taiwan. (corresponding e-mail: peichinlin@ntu.edu.tw).

Here, we report on the development of a kangaroo robot with dynamic gait. Though kangaroo is a biped robot, motions of the legs are usually synchronized. Thus, kangaroo's motion is actually equivalent to a monopod, a very unique class of motion among the overall legged locomotion. Though hopping of the monopod is well researched [8] the SLIP-model-based design of dynamic locomotion is very limited, especially on the aspect of continuous forward motion. Here in this paper we tried the approach of developing dynamic locomotion based on the SLIP-like simplified model. More specifically, the Rolling SLIP (R-SLIP) model is utilized merely because the empirical legs have characteristics of rolling contact, and the scientific concept of methodology is actually the same. The robot COM trajectory is design based on the passive dynamic characteristics of the R-SLIP. In addition, a tail is also installed to compensate the angular momentum and keep the body pitch maintaining in the desired orientation, like the mechanism adopted in kangaroo [9]. The robot is empirically built, and some running experiment is executed to evaluate its locomotion performance.

The rest of this paper is organized as follows. Section II describes the dynamic R-SLIP model and explains how to extract the model analysis to form robot COM motion. Section III describes the usage of tail and its trajectory design method for body pitch compensation. Section IV explains the detailed mechanism design and mechatronic setup, the detail experimental procedures and results are shown in Section V. Finally Section VI concludes the work.

II. Dynamic Motion of the COM

The spring loaded inverted pendulum (SLIP) is widely used as the intrinsic template for legged animals' dynamic locomotion in sagittal plane [10] where the body is treated as a point mass and the legs are represented by a massless linear spring. With the equivalent mapping infrastructure, COM of the robot should move as the point mass and legs of the robot should be driven to act like a single "virtual" spring. The former mapping (i.e., COM motion to point mass motion) is straightforward according to Newtonian Dynamics, except for the existence of the added orientation state associated with the robot body inertia, which will be described in the next session. The latter mapping, however, is more challenge. If a high degree-of-freedom (DOF) leg is utilized as the virtual spring, the design and control of the leg is not a trivial task. In this case, the utilization of a pure springy component as the leg may be realistic. However, it is also difficult to have a reliable and robust linear spring with soft compliant in one direction but rigid in the other one(s). To remedy this challenge, the

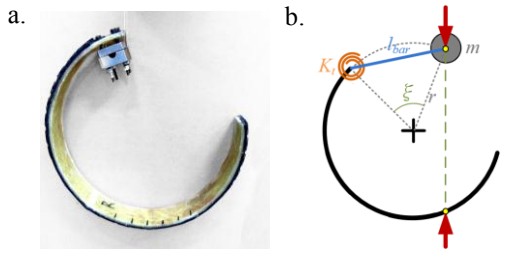

Fig. 1. The half-circular leg of the empirical robot (a) and the R-SLIP model (b).

compliant half-circular material is widely use as the legs of the empirical robots, and the linear spring in the SLIP model is no longer adequate to represent behavior of the empirical leg. Instead, the developed Rolling SLIP (R-SLIP) model is more adequate [11], which has a passive rotational and springy DOF. Two main differences exist between the traditional SLIP model and the R-SLIP model: (i) The former one is point-contact during motion, but the latter one has rolling contact. (ii) The spring stiffness of the former one is fixed, but the equivalent linear spring stiffness of the R-SLIP model varies with the relative position of the contact point with the ground. As a result, the underlying mathematical model is significantly different, and that of the R-SLIP is reviewed [11] in the followed paragraphs for the development purpose.

The composition and the characteristics of the R-SLIP are briefly described in this paragraph. As shown in Fig. 1, it comprises of two parts: the bottom part is a rigid body with arc-shape, and the upper part is a linear rod. Both parts are massless, and they are connected by a torsional spring. The R-SLIP model has four intrinsic parameters: (i) Radius of the half-circular leg, r; (ii) deformation of the torsional spring ξ; (iii) stiffness of the torsional spring, K_t; and (iv) mass of the model, m. Among all parameters, r and m can be captured by robot specification directly. The parameters ξ and K_t can be computed from empirical relationship of force and deformation. With r and ξ, the length of the link l_{bar} can be computed as well. With this method, we can calculate the theoretical values of both location and stiffness of the torsional spring. By comparing theoretical value of the parameters with the measured ones, we can obtain a set of parameters with the least error. In short, the computed K_t of the fiber glass leg on the robot is *16.2 N·m*, and ξ is 72^0.

The dynamic motion of the R-SLIP model is composed of two phases as shown is Fig. 2(a): Stance phase, where leg of the model contacts with the ground, and flight phase, where the model is in ballistic flight. During the stance phase, the torsional spring is compressed which stores the potential energy, and this functionality is like tendon of the kangaroo. When the torsional spring recovers back to its natural configuration, the potential energy changes transforms into kinetic energy the model enters its ballistic flight phase if the resultant velocity of the mass is in the adequate direction. In that case, the only external force acting on the model is gravity. When the R-SLIP model lands on the ground after ballistic flight, the stance phase of the model starts. The

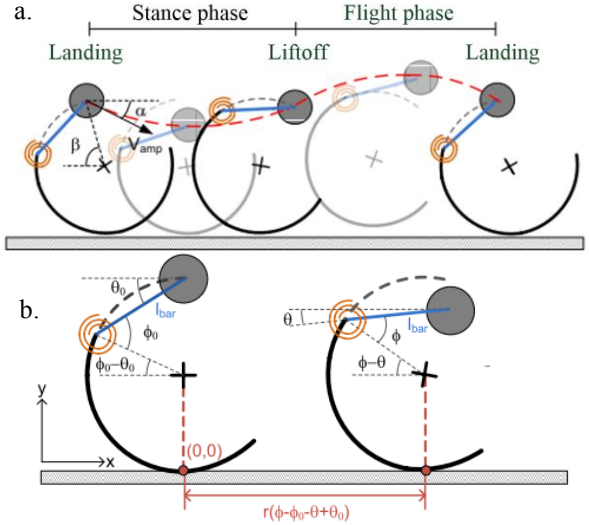

Fig. 2. The R-SLIP model: (a) dynamic motion, and (b) notations for model development.

dynamic behavior of the model can be derived by the Lagrangian method. As shown in Fig. 2(b), position of the mass can be expressed as the functions of the generalized coordinate θ and ϕ, in conjunction with the some model parameters:

$$\begin{aligned} x_s &= r(\phi-\phi_0-\theta+\theta_0)-r\cos(\phi-\theta)+l_{bar}\cos(\theta) \\ y_s &= r+r\sin(\phi-\theta)+l_{bar}\sin(\theta) \end{aligned} \quad (1)$$

where the subscript $_s$ represents stance phase. The kinetic energy T and potential energy V of the R-SLIP model can then be expressed as:

$$\begin{aligned} T &= m(r^2(1+\sin(\phi-\theta))(\dot{\phi}-\dot{\theta})^2 \\ &\quad +rl_{bar}(\cos(\phi)-\sin(\theta))((\dot{\phi}\dot{\theta}-\dot{\theta}^2)+\frac{1}{2}l_{bar}{}^2\dot{\theta}^2) \\ V &= \frac{1}{2}K_t(\phi_0-\phi)^2+mg(r+r\sin(\phi-\theta)+l_{bar}\sin\theta) \end{aligned} \quad (2)$$

Substituting the above values into the Lagrangian equations

$$\frac{d}{dt}\left(\frac{\partial T}{\partial\dot{\theta}}\right)-\frac{\partial T}{\partial\theta}+\frac{\partial V}{\partial\theta}=0\ ,\ \frac{d}{dt}\left(\frac{\partial T}{\partial\dot{\phi}}\right)-\frac{\partial T}{\partial\phi}+\frac{\partial V}{\partial\phi}=0 \quad (3)$$

The equations of motion can be expressed as

$$\begin{bmatrix} a_1(\theta,\phi) & b_1(\theta,\phi) \\ a_2(\theta,\phi) & b_2(\theta,\phi) \end{bmatrix}\begin{bmatrix} \ddot{\theta} \\ \ddot{\phi} \end{bmatrix}=\begin{bmatrix} c_1(\theta,\phi,\dot{\theta},\dot{\phi}) \\ c_2(\theta,\phi,\dot{\theta},\dot{\phi}) \end{bmatrix}, \quad (4)$$

where a_1, a_2, b_1, b_2, c_1, and c_2 represent the functions of the state variables in the parenthesis. The overall motion of the R-SLIP model can be constructed by alternating composition of (1) and (4) with correct initial and final conditions as the bridging elements.

The initial conditions (I.C.s) of the R-SLIP model can be represented by three physically-meaningful parameters as shown in Fig. 2(a): magnitude and angle of the touchdown velocity (V_{amp}, α) as well as landing angle (β), which is the angle included by horizontal line and line segment connecting the mass and center of the circular rim. The adequate set of initial conditions for R-SLIP running is judged based on the stability properties of the model with that specific set of I.C.s.

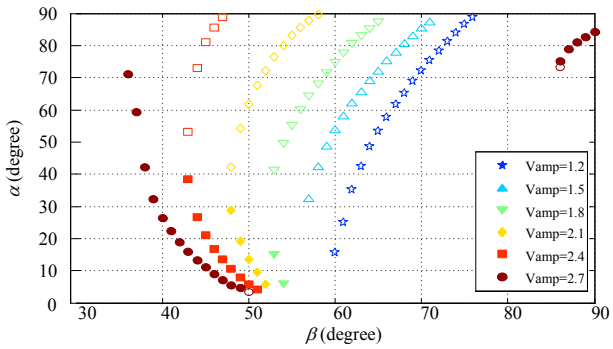

Fig. 3. Basin of attraction analysis of the R-SLIP model with adequate range of valuables for implementation on the physical robot.

The basin of attraction analysis is used, and the original analysis reported in [12] is reevaluated with the correct range achievable by the physical robot. Fig. 3 plots the results of the analysis. The x-axis and y-axis represent the angle of touchdown velocity and landing angle, respectively. Different curves with different colors represent the result of the model with different touchdown speeds. The filled and hollow legends represent stable and unstable fixed points. For the former case, the models with nearby operating conditions converge to the state of those points. In contrast, in the latter case the models with nearby operating points do not converge to the state of those points. In the ideal world, if the robot is operated with the state of stable fixed points, the robot can stably run without any energy input. In reality, the system is hard to be energy conservative, so the energy input to the system is usually required. Thus, in the empirical setting, the motor power is introduced to rotation the "virtual leg," and in this case the motor's capability becomes one of the important issues for choosing adequate operating point. The point must locate within the achievable range of the motor. Fig. 3 reveals that the stable fixed points only exist when the touchdown speed v_{amp} is larger than 1.5 *m/s*. In addition, the selectable points in v_{amp} = *1.8 m/s* is limited, and the number of points increases when the touchdown speed increases. Unfortunately, after empirical testing of the balance between the output torque and output speed, the practical operating speed of the motor on the robot is *1.5 m/s*. In this case, the angle of touchdown velocity should be above 32^0. After checking with kangaroo's running behavior, a similar setting is chose, $\alpha=44^0$, which determines the corresponding landing angle $\beta=58^0$. Because the robot has motor power input, the operation region can be adjusted within the desired domain. After determination of the I.C.s, other quantitative characteristics of the model can then be calculated by using equations of motion shown in (1) and (4), which yields stance-phase time *0.145 s*, flight-phase time *0.186 s*, and lift-off angle *-11.52°*. The theoretical period of the model within this setting is *0.33 s*. List of parameters for R-SLIP model derivation is shown in the upper part of Table I.

Dynamic motion of the R-SLIP model is highly nonlinear, which constraints the possibility of solving equations of motion in real-time by the operation system with limited

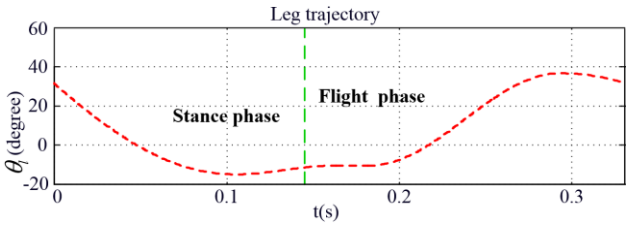

Fig. 4. The trajectory of leg derived by the theoretical model mentioned in Section II. The pair of I.C.s is: V_{amp}=*1.5 m/s*, α=*44°*.

TABLE I
ACTUAL VALUE OF MODEL PARAMETERS

R-SLIP Model		Tail Dynamic Model	
m	5.400 kg	m_b	4.606 kg
r	0.100 m	m_l	0.423 kg
ξ	72.0 °	m_t	0.371 kg
K_t	16.2 N·m	r_b	0.017 m
l_{bar}	0.118 m	r_l	0.090 m
		r_{th}	0.120 m
		r_{tv}	0.177 m

computation recourses on the robot. To remedy this limitation, the motion of the R-SLIP model is approximated by the fifth-order polynomials (i.e., six coefficients, a_0, a_1…, and a_5). In addition, a discrete database with a wide range of different I.C.s is also generated offline and stored in the onboard memory. Thus, not only the selected motion, the motion within the neighborhood settings of the I.C.s can also be tested for empirical performance evaluation. Besides six parameters of the polynomial coefficients, four other important motion parameters are also stored, including stance-phase time, flight-phase time, lift-off angle, and landing angle. In short, ten scalar parameters are stored for each I.C. setting. Fig. 4 shows the desired COM trajectory versus time as the exemplary of the database. During the stance phase, the fifth-order polynomial is implemented to fit the R-SLIP model. During the flight phase, the leg will first decelerate to zero velocity, and then smoothly move to a slightly upper position relative to the initial position by following a cosine curve trajectory. Next, the leg moves down to the initial position of the stance phase with acceleration. By doing so, the velocity discontinuity of the leg between the flight phase and the stance phase can be reduced. Generally, the leg will be held still for a short period of time in the very beginning of lift-off. This setup can prevent the leg from colliding the ground when the flight height is insufficient for the leg to move forward.

III. TAIL MOTION GENERATION

With right motion planning described in the last section, the robot in principle can initiate its R-SLIP-like dynamic locomotion. However, one major discrepancy between the planar world of the R-SLIP model and the empirical robot exists: the latter one has an extra DOF of body pitch since in reality the robot body can hardly be approximated by a point mass. Owing to this reason, the pitch should be regulated, or its variation may result in the wrong leg trajectory versus time,

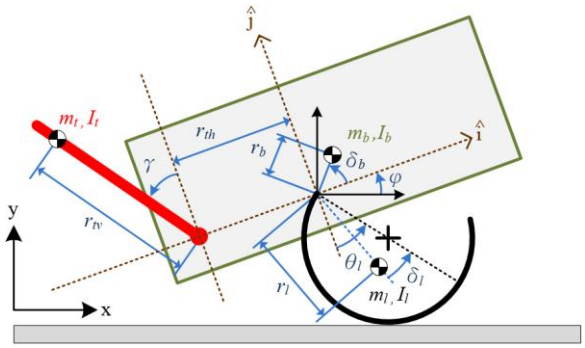

Fig. 5. Sketch of the robot model in sagittal plane with symbols for dynamic equation derivation.

which deviate the COM motion of the robot from the desired R-SLIP-like motion. In that case, the robot may fail to run after several strides. Therefore, the robot should equip with a mechanism which can regulate the body orientation change, and an active tail is adopted, as bio-inspired from the morphology of kangaroo.

The robot tail is designed to keep the body pitch maintaining horizontal posture. During the stance phase, the robot leg in principle should be moved purely according to passive dynamics without motor input. In contrast, the leg has to be driven back for the next landing by motor power. Because the robot leg is driven by the motor mounted on the body, the forward leg motion of the robot during its flight phase generate re-active torque to the robot body. In addition, COM position also varies because of movement of the leg (and the tail). When the COM does not locate at the hip joint where the leg is mounted, the gravity also generates an unwanted torque to the body. These two factors cause undesirable change of the body pitch during the flight phase. Thus, the tail motion is designed to compensate the effects caused by these two factors, adjusting the body pitch back to 0°. As a side note, by checking with the kangaroo running, we believe that the tail is used to balance the angular momentum caused by legs' swing motion. Therefore, motion of the tail in the flight phase is derived based on the conservation of the angular momentum.

Quantitative derivation of the tail motion is described as follows. With the symbols defined in Fig. 5, the equation which conserves angular momentum of the body, the leg, and the tail can be expressed as:

$$\begin{aligned} &-gm_l r_l \sin(\theta_l+\varphi-\delta_l) \\ &-gm_b r_b \cos(\varphi+\delta_b)+gm_t(r_{th}+r_{tv}\sin(\varphi+\gamma)) \\ &=I_b\ddot{\varphi}+I_l(\ddot{\theta}_l+\ddot{\varphi})+I_t(\ddot{\gamma}+\ddot{\varphi}) \end{aligned} \quad (5)$$

which can further be described in the state-space form:

$$\frac{d}{dt}\begin{bmatrix}\gamma\\ \dot{\gamma}\end{bmatrix}=\begin{bmatrix}\dot{\gamma}\\ C(\theta_l,\varphi,\gamma,\theta_l,,\ddot{\varphi})\end{bmatrix} \quad (6)$$

with

$$\begin{aligned} C(\theta_l,\varphi,\gamma,\theta_l,\ddot{\varphi}) = [&-gm_l r_l \sin(\theta_l+\varphi-\delta_l)-gm_b r_b \cos(\varphi+\delta_b) \\ &+gm_t(r_{th}+r_{tv}\sin(\varphi+\gamma))-(I_b+I_l+I_t)\ddot{\varphi}-I_l\ddot{\theta}_l]/I_t \end{aligned}$$

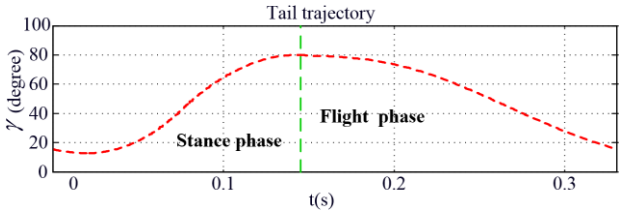

Fig. 6. The trajectory of tail derived by the theoretical model mentioned in Section III. The pair of I.C.s is: flight phase time = *0.186 s*, landing foot angle = *44.017°*, lift-off foot angle = *-11.52°*, and lift-off pitch = *0°*, respectively.

where φ represents body pitch, and θ_l represents the orientation of the leg with respect to the body coordinate with zero defined when the leg is posed vertically. The parameters δ_b and δ_l defines relative configurations the body COM and the leg COM. The symbols m and I represent mass and inertia, respectively. The subscripts $_b$, $_l$, and $_t$ represent body, leg, and tail, accordingly. The symbol γ represents the orientation of the tail with respect to the body. Note that leg motion and tail motion are both defined with respect to the body because they are driven by the motors mounted on the body; thus the relative definition is easier for empirical motion control. Because the leg axis and the tail axis do not coincide at the same axis, the offset r_{th} and r_{tv} have to be considered separately. By using (6) with the I.C.s, the trajectory of the tail versus time can be quantitatively yielded by the numerical method, similar to that of the leg motion. In conclusion, list of parameters for tail model derivation is shown in the lower part of Table I.

Trajectory of the tail is affected by four variables: flight-phase time, leg landing angle, leg lift-off angle, and lift-off body pitch. The first three variables can be directly obtained from the R-SLIP database described in the previous section because in principle the actual leg trajectory agrees with that of the R-SLIP model. Regarding the last one, there are two different circumstances where we can acquire the pitch data: If open-loop, the pitch is manually set to a suitable value, and if closed-loop, it can be estimated by an onboard sensor with state-deriving algorithm.

Similar to the leg motion, dynamic motion of the tail motion is also highly nonlinear. Therefore, the same online trajectory generation method is also applied to the tail trajectory in the flight phase, which is approximated by a fifth-order polynomial. As for the stance phase, the tail gradually slows down and then smoothly moves back to the initial position of flight phase by following a cosine curve trajectory. For each set of I.C.s, six coefficients of the polynomial (b_0, b_1…, and b_5) are derived. Together with the other two parameters (flight-phase time, stance-phase time), formation of the entire tail trajectory is completed, where Fig. 6 shows an exemplary trajectory.

IV. Robot Design and Mechatronic Infrastructure

In order to make the actual movement of the empirical robot coherent to the movement of the reduced-order R-SLIP model, several design considerations should be accounted for.

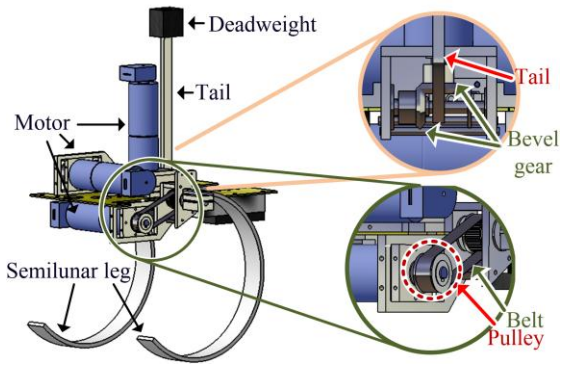

Fig. 7. CAD drawing which shows transmission mechanism of the robot.

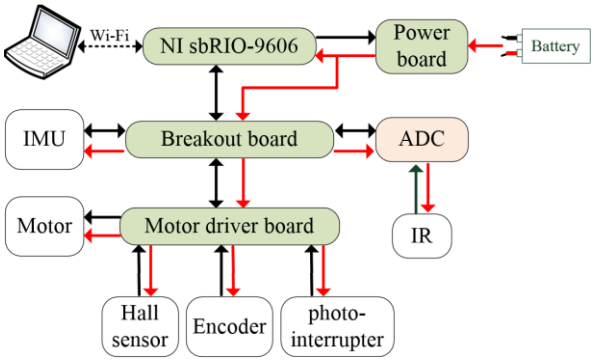

Fig. 8. Mechatronics of the robot. (The black arrows indicate the direction of the signal, whereas the red arrows indicate the direction of the current)

(i) First, discrepancy between numbers of the legs: Only one virtual leg exists in the planar R-SLIP model, but the robot, like the kangaroo, has two legs. Though in this research the two legs move synchronically, it cannot be reduced to single leg movement since the undesirable roll angle of the robot during jogging will occur unavoidably by the mere presence of the single-leg design. This discrepancy raises the issue of motor arrangement. Though in the simplified setup two legs can be driven by one motor (which also good for motion synchronization), in the final version two legs are driven individually because this arrangement provides the possibility of turning by using phase difference. (ii) Second, tight space around the hip area: From equation point of view, rotational axis of the tail should coincide with hip of the leg because in this case the dynamic model is simpler than that of the non-coincided design. This implied that three motors should transmit their powers to a line which passes the hip and is orthogonal to the sagittal model plane, and the final mechanism arrangement is shown in Fig. 7. The motor for the tail is posed vertically and shifted a little backward for weight distribution, and its rotational motion is transmitted to the right direction through a pair of bevel gear. Rotational axis of the tail is designed to be movable, allowing adjustment of the COM position of the overall robot. In addition, because the middle space is taken by the tail motor, the leg motors are placed paralleled to the hip axis, and their power is transmitted back to the hip axis through pulley-and-belt systems. This design also provides the possibility for quick adjustment of the transmission ratio by changing pulley's numbers of teeth. (iii)

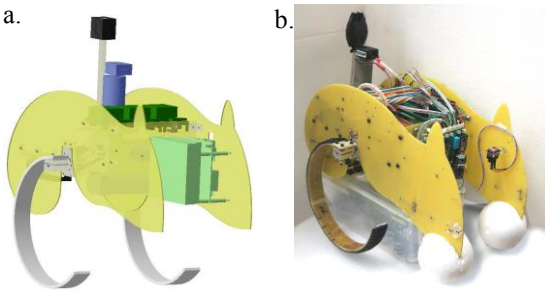

Fig. 9. The CAD drawing (a) and the photo (b) of the robot.

TABLE II
SPECIFICATIONS

Robot Information	
Mass	5.4 kg
Length	0.460 m
Width	0.265 m
Height	0.240 m

Change of tail configuration: Instead of orienting toward back side as the nominal configuration, the tail is oriented *45°* up. In this configuration, the motion range of the tail is within vertically up and horizontally toward back side; thus reducing the chance of collision between the tail and the ground when the body pitch is varied. In addition, the mechanical stops on both ends are also designed for operation safety. (iv) Material of the robot: Structure of the body is made by composition of light-weight commercial fiberglass composites. In contrast, the legs are custom-made in order to create adequate stiffness, and the photo of the leg is shown in Fig. 1(a).

Regarding the mechatronic system, the robot has a real-time embedded control system (sbRIO-9606, National Instruments) operating at 500Hz loop rate, together with an integrated field programmable gate array (FPGA) for high-speed signal exchange, such as pulse width modulation (PWM)-based DC motor control, analog-to-digital converter (ADC), and SPI interface for inertial measurement unit (IMU) readings. The remote operator can communicate with the embedded system on the robot through 802.11b wireless standard, giving high-level motion command and receiving the sensory information. The sbRIO-9606 connects to a custom-designed breakout board, which further connects to various sensors and three actuators with motor driving boards. Two hall sensors (42A, Honeywell) are installed for absolute leg orientation calibration, and one photo interrupter (CNZ1023-DN, Panasonic) are mounted to define the motion boundary of the tail. A six-axis IMU (ADIS16364, Analog Devices) is approximately mounted at COM. Two infrared distance sensors (GP2Y3A001K0F, Sharp) are mounted on the bottom side of the robot, measuring the distance between the body and the ground for pitch measurement. Their analog signals are converted to digital signals through an ADC (MCP3208, Microchip). An illustrative drawing of the mechatronic system is shown in Fig. 8. A CAD drawing and a photo of the robot are shown in Fig. 9. Some major specifications of the robot are listed in Table II.

V. EXPERIMENTS AND ANALYSIS

Performance of the designed robot described in Section IV was experimentally evaluated. The robot was programmed to track the designed COM and tail trajectories described in Section II and Section III, respectively. Fig. 10(a) plots the sequential snapshots of one trial with several running strides. Three markers were installed on one side of the robot, where the camcorder faced. When the camcorder recorded the motion of the robot, robot COM captured in the sequential images could be extracted and calibrated to be represented in the planar displacement. The COM planar trajectory associated with the experiment shown in Fig. 10(a) is drawn in Fig. 10(b). In reality, because the non-perfect environmental setting or the unexpected disturbance entered the system, the robot might not move according to its nominal trajectory designed based on the R-SLIP model. In that case, the motor indeed provided certain power output to regulate the leg motion. As a result, the extra torque acted on the leg also generated the re-active torque on the body, which made the robot body had pitch variation. The resultant torque kept accumulating and caused the body head-up in the stance phase. As a result, the body entered the followed flight phase with unwanted body pitch. The body pitch remained the same during the flight phase, but the next stance phase might also add extra pitch. With this gradually increased body pitch, the robot failed after several strides. As a result, the tentative solution to remedy this accumulated error is to mount two external strings on both sides of the robot, which helped to calibrate the body pitch back to the consistent condition at the lift-off moment. By carefully checked the sequential images recorder by the camcorder, we found that the strings interfered with the system about 5% time in each stride, which made the experimental setup was not perfect but tolerable. With this add, the robot could run continuously. The automatic body pitch adjusting system requires onboard pitch estimation and associated real-time pitch regulation strategy, which is currently under investigation. The experimental results also confirm the advantage of the tail motion.

VI. CONCLUSION

We report on the development of a kangaroo robot with dynamic locomotion. Taking advantage of the kangaroo's monopod running behavior, the inverted pendulum based dynamic model is applied as the motion model of the robot. Thus, like how kangaroo moves, two legs of the robot run synchronically, resulting simplification of the robot's original spatial motion into planar one. The sagittal planar motion of the real robot has three DOFs. The translation DOFs of the robot is mapped to the motion of the SLIP model, where the R-SLIP model is utilized owing to the rolling characteristics of the empirical robot legs. The trajectories are determined by the physical characteristics of the robot and the adequate selection of the initial conditions. The remaining body orientation DOF does not included in the model, so the separate treatment to keep its stability is necessary. In this work, the tail is implemented to balance the leg retraction during the flight phase, thus decreasing the unwanted pitch variation. The proposed system setup and locomotion strategy is realized on the real robot and evaluated experimentally. The results shows that the tail is effective and the robot can run for several strides, but the system is yet to be reliable enough to perform stable running for a long period of time, which might requires a dedicate and effective online pitch regulation strategy.

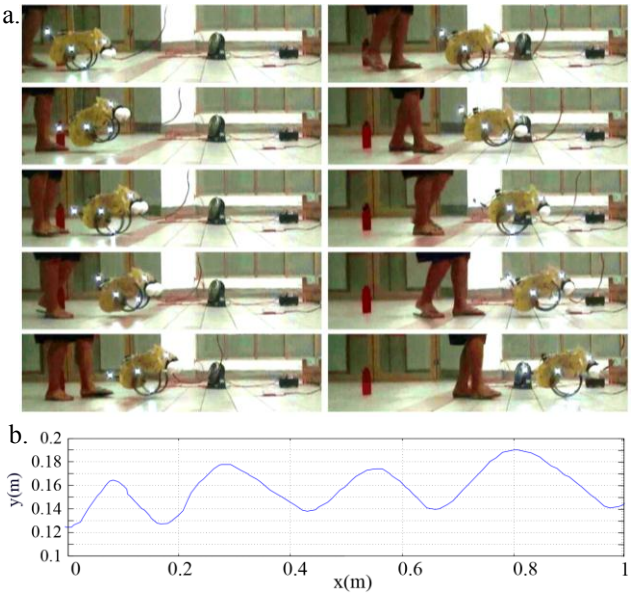

Fig.10. The actual planar COM trajectory recorded by a camera

REFERENCES

[1] M. Raibert, K. Blankespoor, G. Nelson and R. Playter, "BigDog, the rough-terrain quaduped robot," in *Proc. of the 17th IFAC World Congress*, Jul 2008, Seoul, Republic of Korea, pp. 10822–10825.

[2] H. Kimura, Y. Fukuoka, and A. H. Cohen, "Adaptive dynamic walking of a quadruped robot on natural ground based on biological concepts," *International Journal of Robotics Research,* vol. 26, pp. 475-490, May 2007.

[3] I. Poulakakis, J. A. Smith, and M. Buehler, "Modeling and experiments of untethered quadrupedal running with a bounding gait: The Scout II robot," *International Journal of Robotics Research,* vol. 24, pp. 239-256, Apr 2005.

[4] S. Kim, J. E. Clark, and M. R. Cutkosky, "iSprawl: Design and tuning for high-speed autonomous open-loop running," *International Journal of Robotics Research,* vol. 25, pp. 903-912, Sep 2006.

[5] T. A. McMahon, and R. M. Alexander, "Elastic mechanisms in animal movement," *Nature,* vol. 336, pp. 530-530, Dec 1988.

[6] U. Saranli, M. Buehler, and D. E. Koditschek, "RHex: A simple and highly mobile hexapod robot," *International Journal of Robotics Research,* vol. 20, pp. 616-631, Jul 2001.

[7] X. Zhou and S. Bi, "A survey of bio-inspired compliant legged robot designs," *Bioinspiration & Biomimetics,* vol. 7, p. 041001, 2012.

[8] M. Raibert, *Legged robots that balance*: MIT Press, 2000.

[9] C. T. Farley, J. Glasheen, and T. A. McMahon, "Running Srings - apped and animal size," *Journal of Experimental Biology,* vol. 185, pp. 71-86, Dec 1993.

[10] W. J. Schwind, "Spring loaded inverted pendulum running: a plant model," University of Michigan, 1998.

[11] K. J. Huang and P. C. Lin, "Rolling SLIP: A model for running locomotion with rolling contact", in *Proc. IEEE/ASME International Conference on Advanced Intelligent Mechatronics (AIM)*, Jul 2012, Taipei, Taiwan, pp. 21-26.

[12] J. Rummel, and A. Seyfarth, "Stable running with segmented legs," *The International Journal of Robotics Research*, vol. 27, pp. 919-934, Aug 2008.